Space Sci Rev (2010) 152: 543–564
DOI 10.1007/s11214-009-9546-1

Laboratory Dynamo Experiments

Gautier Verhille · Nicolas Plihon · Mickael Bourgoin · Philippe Odier · Jean-François Pinton

Received: 22 March 2009 / Accepted: 29 May 2009 / Published online: 7 July 2009
© Springer Science+Business Media B.V. 2009

Abstract Since the turn of the century, experiments have produced laboratory fluid dynamos that enable a study of the effect in controlled conditions. We review here magnetic induction processes that are believed to underlie dynamo action, and we present results of these dynamo experiments. In particular, we detail progress that have been made through the study of von Kármán flows, using gallium or sodium as working fluids.

Keywords Magnetic fields · Magnetohydrodynamics · Dynamo · Experiments · Instabilities · Turbulence

1 Introduction

Although dynamo research is essentially motivated by observations from planetary and stellar dynamos, the conditions that prevail in such natural objects cannot be reproduced in the laboratory. Experiments and numerics can only be run in quite different parameter regimes, but they both provide useful insights into the features of natural dynamos. Experiments cannot be rotated as fast as real systems do, convective motion cannot be as strong, etc., but they run with real fluids and probe quantities that cannot be accessed from remote observations of natural dynamos. Numerical experiments record the complete dynamical fields in space and time (but at quite removed parameter values) while laboratory experiments probe a limited part of the velocity and magnetic fields ($\mathbf{u}$, $\mathbf{B}$). The two approaches are complementary and have been associated in most recent works. Numerical development are reported in several contributions to this volume. We focus here on the specific issues involved in the actual implementation of an experimental dynamo and recall the findings of recent studies. The reader

G. Verhille · N. Plihon · M. Bourgoin · P. Odier · J.-F. Pinton (✉)
Laboratoire de Physique de l'École Normale Supérieure de Lyon, CNRS & Université de Lyon, 69364 Lyon, France
e-mail: pinton@ens-lyon.fr

M. Bourgoin
Laboratoire des Ecoulements Geophysiques et Industriels, CNRS/UJF/INPG UMR5519, BP53, 38041 Grenoble, France

is also referred to reviews that have recently been published (Magnetohydrodynamics 2002; C.R. Acad. Sci. 2008; Stefani et al. 2008; Pétrélis et al. 2007).

In order for a dynamo to be self-sustained, the production of induced currents by fluid motions must overcome the resistive Joule dissipation. This condition sets an instability threshold, requiring that the magnetic Reynolds number of the flow ($R_M = UL/\lambda$) exceeds a critical value R_M^c (U and L are characteristic velocity and length and λ is the magnetic diffusivity). An energy-based criterion for generation inside a sphere gives a lower bound $R_M^c > \pi^2$. For more complex geometries, and taking into account real flow structure there is no general expression for R_M^c. On the contrary, theorems prevent dynamo action for too simple geometries (Moffatt 1978). Assuming R_M^c values of the order of 10 to 100 (a value often quoted for the Earth), and given the fact that all liquid metals have magnetic Prandtl numbers (ratio of kinetic to magnetic diffusivities) of the order of $P_M \sim 10^{-5}$, one realizes that dynamo flows are associated with huge kinetic Reynolds number values $R_V = R_M/P_M$, typically exceeding 10^6. Such high R_V values are associated with fully developed turbulence, an observation that raises several central issues for dynamo experiments.

Turbulence is often synonymous of (a) disordered motions, and (b) strongly diffusive features. In this context, (a) means that the specific motions that favor dynamo action may be disrupted by the randomness of the flow. In addition, the small magnetic Prandtl number values impose that the Joule resistive scale is very much larger than the hydrodynamic viscous length. It is therefore tempting to perform some kind of sub-scale average of the action of the turbulent velocity field. Then (b) leads to an effective magnetic diffusivity that could be much larger than the molecular value. These considerations have raised doubts on the very existence of fully turbulent dynamos (Schekochihin et al. 2004).

One alternative is to engineer flow configurations that will preserve flow patterns which are essential for the dynamo generation. The design of the Riga and Karlsruhe experiments have been made to ensure that the time-averaged flow field resembles laminar flow that are kinematic dynamo solutions (Magnetohydrodynamics 2002; C.R. Acad. Sci. 2008). These pioneering studies have validated the principle of a *fluid* dynamo, and have shown many fundamental dynamo properties. The threshold for dynamo action has been found to be in good agreement with predictions, showing the predominance of the large scales in their dynamo processes.

Another possibility, often explored in the geophysics community, is provided by strongly rotating flows. In this case, the Proudman-Taylor constraint may be able to prevent the development of strong three-dimensional turbulent fluctuations. This effect may even be strengthened by the generation of a dynamo dipole with its axis parallel to the rotation vector. Experiments in rotating Couette flows are studied in Grenoble (Schmitt et al. 2008) and Maryland (Sisan et al. 2004). Preliminary studies have not shown self-generation, but have pointed to the existence of *waves* in these strong rotating and magnetized flows: inertial, magneto-rotational, Alfvèn, etc. The role of these waves regarding dynamo self-generation has yet to be elucidated.

The VKS experiments have shown that it is possible to generate a dynamo from fully turbulent motions. Its characteristics have not been predicted by studies based on the time-averaged flow pattern, although it is believed that helicity and differential rotation do play a leading role. The existence of fully turbulent motions has a major impact on the power requirement of the experiment. In the limit of very high R_V values, the hydrodynamic power consumption (below dynamo threshold) scales as $P = \rho L^2 U^3$ (ρ is the fluid density), leading to magnetic Reynolds number $R_M = \mu\sigma(PL/\rho)^{1/3}$ (μ and σ are the magnetic permeability and electrical conductivity of the fluid, so that $\lambda = 1/\mu\sigma$ is its magnetic diffusivity). Engineering difficulties typically scale with the size L of the experiment, while operational

costs are best associated with the power input P. Then, the above scaling shows that in order to reach high R_M values, one should use a fluid with the best electrical conductivity and lowest density (hence the use of liquid sodium), with size and power consumption only contributing to the one-third power. $R_M \sim 10$ requires power inputs of the order 100 kW. As a result, it is easily realized that highly overcritical regimes will not be achieved in laboratory studies using conventional fluids (Spence et al. 2009): experiments aim at reaching for the neighborhood of the threshold for dynamo onset. In addition, it implies that once a geometry has been chosen, small variations in R_M^c can have a huge impact on the power or the size of the flow needed to reach self-generation. As a result, all experiments have been thoroughly optimized to have the lowest possible critical magnetic Reynolds number. This is a noteworthy peculiarity of the study of this hydromagnetic instability: energy and engineering constrains are such that one is not able to increase at will the control parameter of the instability; one must also choose conditions such that the threshold is within the capacity of the selected setup. In this respect, the details of flow entrainment and the adjustment of boundary conditions have been essential to all dynamo experiments so far.

We will first review the main induction processes that have been evidenced in fully turbulent MHD flows, before discussing the findings of dynamo experiments. We illustrate most features using measurements in the swirling flow generated in the gap between coaxial impellers inside a cylinder—the von Kármán flow geometry, which we have studied using gallium or sodium as working fluid.

2 Magnetic Induction and Dynamo Issues

Magnetohydrodynamics solves the coupled set of induction and momentum equations:

$$\partial_t \mathbf{B} = \nabla(\mathbf{u} \times \mathbf{B}) + \lambda \Delta \mathbf{B}, \tag{1}$$

$$\partial_t \mathbf{u} + (\mathbf{u} \cdot \nabla)\mathbf{u} = -\frac{\nabla p}{\rho} + \nu \Delta \mathbf{u} + \frac{\mathbf{j} \times \mathbf{B}}{\rho} + \mathbf{f}, \tag{2}$$

where $\lambda = 1/\mu_0 \sigma$ is the magnetic diffusivity of the fluid with density ρ, $\mathbf{j}$ the electrical current, and $\mathbf{f}$ is the forcing term (which may include Coriolis or buoyancy forces if rotation/convective effects must be included). Flows of liquid metals as considered in the experiments discussed here are incompressible so that the velocity and magnetic fields are divergence free. Boundary conditions correspond to no-slip for the hydrodynamic field (the velocity at the boundary is equal to the velocity of the boundary), with the magnetic boundary conditions set by the characteristics of the boundary (electrical conductivity σ_b, magnetic permittivity μ_b). Magnetic boundary conditions can be implemented by setting continuity conditions at the surface, e.g. $[\mathbf{n}.\mathbf{B}] = 0$, $[\mathbf{n} \times \mathbf{H}] = \mathbf{j}_s$ where $\mathbf{n}$ is the normal to the surface, $\mathbf{j}_s$ are eventual surface currents and [.] stands for 'jump across the surface'. Alternatively, the induction equation can be extended to the entire domain (encompassing regions outside the flow—with the condition that $\mathbf{B} \to 0$ at infinity), and inhomogeneities are incorporated into Ohm's law:

$$\nabla \times \frac{\mathbf{B}}{\mu(\mathbf{r})} = \sigma(\mathbf{r})(\mathbf{E} + \mathbf{u} \times \mathbf{B}), \tag{3}$$

where the magnetic permeability and electrical conductivity depend on position. Taking the curl of the above equation yields the induction equation in an inhomogeneous medium:

$$\partial_t \mathbf{B} = \nabla \times (\mathbf{u} \times \mathbf{B}) + \lambda \Delta \mathbf{B} + \nabla \times (\lambda \nabla \ln \mu \times \mathbf{B}) - \nabla \lambda \times (\nabla \times \mathbf{B}) \tag{4}$$

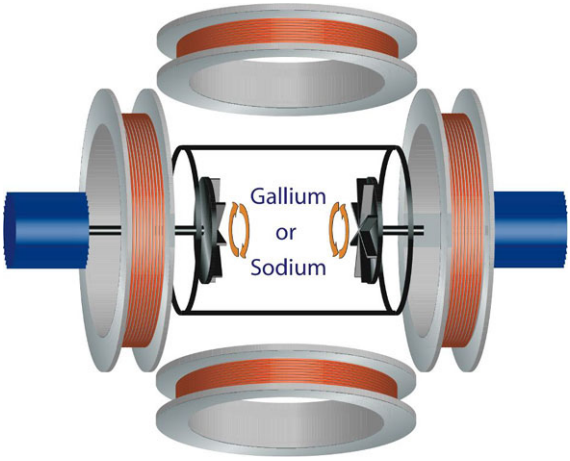

Fig. 1 Schematics of induction measurements in the von Kármán geometry (Zandbergen and Dijkstra 1987). Flows are generated by the independent rotation of 2 coaxial impellers (co- or counter-rotating) in a cylinder—the aspect ratio is one, with a cylinder diameter equal to the distance between the impellers. Depending on the configurations, the resulting mean flows have azimuthal and meridional profiles similar to the $s_{1,2}t_{1,2}$ types considered by Dudley and James (1989) for dynamo generation. Note that these flows are strongly turbulent (Mordant et al. 1998; Pinton et al. 1998; Volk et al. 2006b); discussions in this section are restricted to the mean (time-averaged) features. External coils are set to apply either axial or transverse fields, and Hall probes inserted inside the flow vessel allow the measurement of the magnetic fields induced by the fluid motions

with $\lambda = 1/\mu\sigma$, and it will be pointed out below that boundary conditions are essential for the interpretation of measurements of magnetic induction (Bullard and Gubbins 1977; Moffatt 1978; Bourgoin 2003).

2.1 Induction Processes

Despite efforts that are now almost a century old, research has so far failed to establish sufficient conditions for dynamo action—some necessary conditions have been provided by anti-dynamo theorems. In this context, work has been aimed at uncovering efficient induction processes that could co-operate towards dynamo generation. In these studies an external field $\mathbf{B}^A$ is applied, and one analyses magnetic response, *i.e.* the induced field $\mathbf{B}^I$. For simplicity, the applied field is often homogeneous. We review in this section essential mechanisms that have been uncovered, with examples drawn from our own studies of the von Kármán flows generated inside a cylinder by the rotation of coaxial impellers, cf. Fig. 1. In these studies the applied field is low, so that the effect of the Lorentz force can essentially be neglected in the fluid momentum equation. The magnetic response probes the structure of the velocity gradients and boundary conditions.

2.1.1 Shear and ω-effect

One mechanism is the shearing of magnetic field lines by velocity gradients, *i.e.* with $\mathbf{B}^I$ having its source in the $B^A\partial_A\mathbf{v}$ term of the induction equation, where $\partial_A\cdot$ stands for 'gradient along the A-direction'. For steady state conditions at low magnetic Reynolds number, the induction equation then leads to a linear dependence of B^I with R_M, a feature that can be used to estimate an intrinsic magnetic Reynolds number from experimental data as

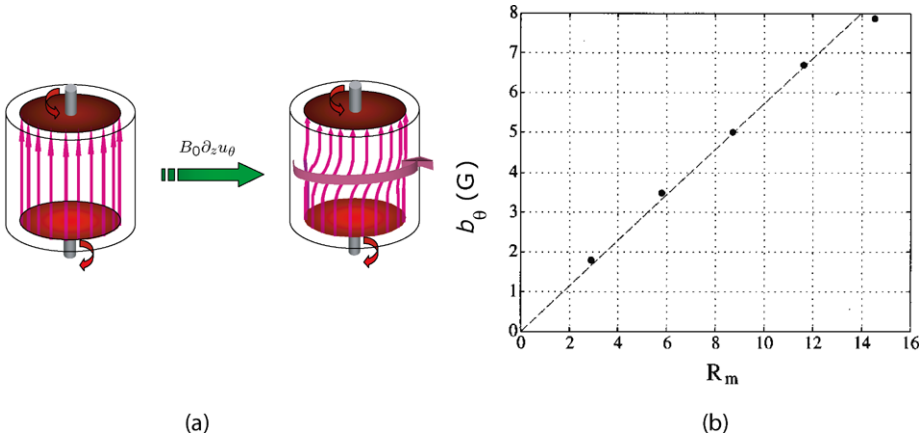

Fig. 2 Experimental verification of ω-effect in the von Kármán flow. Gallium is the working fluid. An axial magnetic field is applied with external Helmholtz coils, and the azimuthal induced field is measured by a Hall probe in the mid-plane and inside the flow. Applied field 33 G. (**a**) Sketch of the effect; (**b**) measurement of the induced field with $R_M = 2\pi R^2\Omega/\lambda$—where R is the radius of the cylindrical vessel and Ω the rotation rate of the impellers. Plot from Odier et al. (1998)

$R_M^I \equiv B^I/B^A$ (Martin et al. 2000). This induction process is called the ω-effect when the velocity gradient comes from differential rotation, *e.g.* from a variation of a rotation rate along its axis. An example is provided in the von Kármán setup when the flow is driven by counter rotation of the impellers. A layer with differential rotation forms in the mid-plane and the twisting of axially applied magnetic field lines generates an azimuthal component—cf. Fig. 2.

Another simple instance of this situation is when an electrically conducting plate rotates above a similar one at rest: if an external field is applied parallel to the axis of rotation, the differential rotation generates an induced field in the azimuthal direction. The solid rotor dynamo experiment devised in the 1960s by Lowes and Wilkinson is based on this principle (Lowes and Wilkinson 1963, 1968): it couples two such induction effects in an 'ω^2-dynamo'.

2.1.2 Helicity and the 'Parker-Effect'

Another crucial mechanism is the 'stretch and twist' effect (Parker 1955): helical motions can deform initially straight magnetic field lines into loops which are associated with induced currents parallel to the applied field, $\mathbf{j}^I \propto \mathbf{B}^A$. This non-linear effect was first tested experimentally by Steenbeck et al. (1968) in an arrangement with interlaced channels—note that in this original setup the local helicity $h = \mathbf{u} \cdot (\nabla \times \mathbf{u})$ is strictly zero everywhere, so that the magnetic field diffusion is essential in this process.

This Parker-effect has also been observed directly in von Kármán experiments (Pétrélis et al. 2003; Bourgoin et al. 2004a): the flow is generated inside a cylinder by the rotation of one disk at one end of the cylinder; it acts as a centrifugal pump so that fluid is drawn in a swirling motion along the cylinder axis. As expected the induced magnetic field varies quadratically with the flow velocity, $B^I \sim B^A R_M^2$ (dashed line in the measurements of Fig. 3). However, at high R_M another effect sets in: the expulsion of the applied field from coherent eddies (see below) which causes a saturation in the Parker-induced magnetic field.

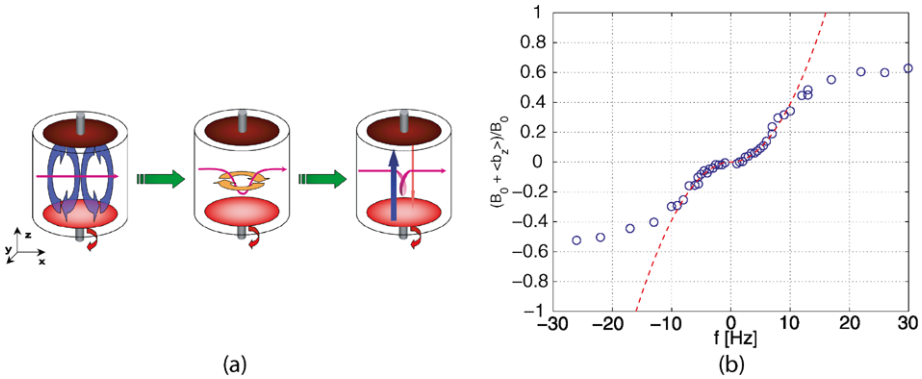

Fig. 3 Experimental verification of the Parker-effect in the von Kármán sodium flow. A magnetic field perpendicular to the cylinder (along the x-axis) is applied with external coils and the axial component of induced field is measured by a Hall probe inserted in the mid-plane, inside the flow. (**a**) Sketch of the effect; (**b**) measurement of the induced field variation with the rotation rate of the impellers, from Pétrélis et al. (2003). The *dashed* (*red*) *line* is a quadratic fit; departure at large rotation rates (> 10 Hz) is due to the expulsion of the applied field by the flow rotation

2.1.3 Coherent Vortex Motion and Expulsion

Rotational flow motion was involved in the two above examples of ω and Parker effects. However, another well-known effect is the expulsion of magnetic field lines from regions with closed streamlines (Moffatt 1978) (Chap. 3). If a magnetic field is initially applied transverse to a coherent vortex, then closed loops form and decay in such a way as to gradually expel all magnetic flux from any region in which the streamlines are closed. This effect is related to the traditional skin penetration of conventional electromagnetism (in the reference frame rotating with the vortex). It is has been clearly evidenced in the von Kármán swirling flow with the impellers *co-rotating* so as to generate a coherent axial vortex (Simand et al. 2000).

A sketch of the effect and corresponding experimental measurements are shown in Fig. 4, taken from Odier et al. (2000). The field decays near the rotation axis, and correspondingly field lines are compressed outside of the vortex core. This effect has also been clearly observed during the growing stage of the Riga dynamo: the Earth magnetic field is first expelled from the swirling motion (Gailitis et al. 2003) and then the dynamo field grows.

2.1.4 Electrical Boundary Conditions

Boundary conditions play an important role, particularly in the way induced currents flow in the system. As a result, induced magnetic fields measured by a local probe come from an overall distribution of induced currents rather than from a local deformation of applied magnetic field lines. This can be clearly illustrated again using the von Kármán geometry with counter-rotating impellers and a transverse applied field—Fig. 5(a1). The deformation associated with differential rotation corresponds to an axial current sheet in the mid-plane, as in Fig. 5(a2, 3). In turn, these currents generate induced field near the insulating boundary (shown in Fig. 5(a4)) at a right angle from the applied field (Bourgoin 2003; Bourgoin et al. 2004a).

This effect, which we term the 'BC-effect', has its origin in the $\nabla\lambda \times (\nabla \times \mathbf{B})$ term in (4). It varies linearly with the magnetic Reynolds number as does its source—the dif-

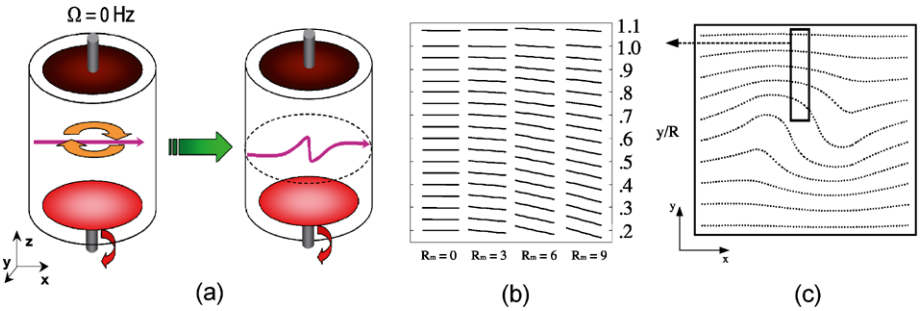

Fig. 4 Experimental verification of magnetic expulsion by coherent vortex motions. Gallium is the working fluid. A uniform magnetic field perpendicular to the cylinder (along the x-axis) is applied with external coils and the evolution of its orientation along a radius is studied as the magnetic Reynolds number is increased. (**a**) Sketch of the torsion of the applied field lines; (**b**) evolution of magnetic field orientation in the measurement (the lines give the local direction of the magnetic field inside the vessel), from Odier et al. (2000); (**c**) equivalent numerical simulation at $R_M = 20$ from Weiss (1966). The boxed region is the one probed experimentally in (**b**), at increasing R_M values

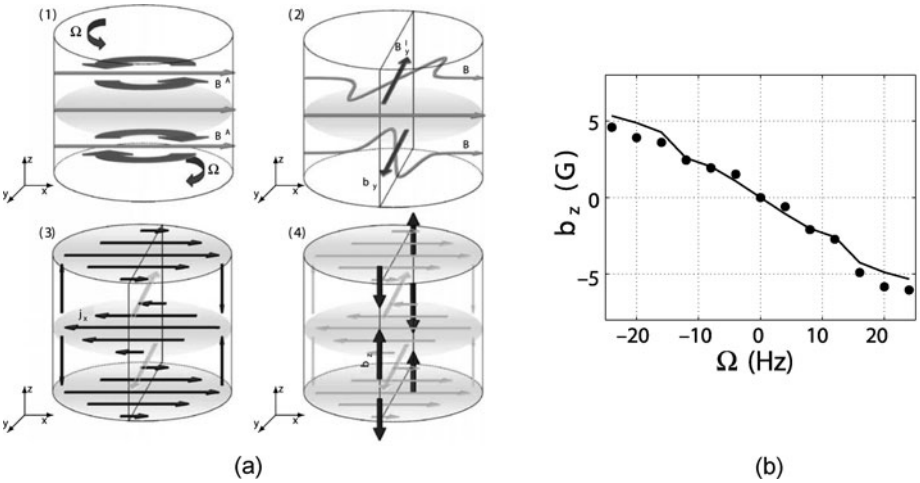

Fig. 5 Effect of boundary conditions. (**a**) Sketch of the BC-effect for a transverse applied field (33 gauss) B^A along the x-axis in a counter rotating von Kármán flow: (**1**) initial field and discs rotations; (**2**) differential rotation creates an induced component B_y; (**3**) induced current sheets responsible for the generation of B_y; (**4**) axial field B_z generated at the wall $y = R$, due to the discontinuity in electrical conductivity. (**b**) Measurements of the induced axial magnetic field by BC-effect for a transverse applied field along the x-axis with both counter-rotating discs in von Kármán experiment, from Bourgoin et al. (2004a)

ferential rotation, and the effect has been accurately treated in several numerical simulations (Bourgoin et al. 2004b; Stefani et al. 2006; Xu et al. 2008). Inhomogeneities in the magnetic boundary conditions, which appear to favour dynamo action (Monchaux et al. 2007) have been considered in numerical studies (Avalos-Zuniga and Plunian 2005; Gissinger et al. 2008) but need to be probed in more details experimentally.

2.1.5 Discussion

The above induction mechanisms have been the building blocks of dynamo experiments so far—and this has motivated their presentation. A detailed discussion of induction in MHD is outside the scope of this review, but the following remarks may be helpful in regards to experimental investigations:

- At low R_M, induction is linear in the velocity gradients and can thus be used to probe them. This is a very useful feature for the study of hydrodynamics in liquid metals, for which velocimetry techniques are not as well developed as for conventional liquids. For instance, it has recently been used in the Grenoble and Maryland experiments for the study of waves in spherical Couette flows (Kelley et al. 2007; Schmitt et al. 2008).
- Induction from uniform applied field may mask non-local features of the induction process, for which magnetic field advection is as important as line deformation. In addition, the presence of the Laplacian term in the induction equation performs some kind of averaging since at low P_M the resistive scale is much larger than the turbulence viscous cut-off. Advection effects from localized magnetic field sources have been studied in the VKS experiment (Volk et al. 2006a); field transport can reach distances larger than the flow integral scale and cause significant magnetic intermittency when turbulence is present.
- It has been observed in several instances (cf. Gailitis et al. 2000; Ravelet et al. 2007) that the induced magnetic field within the flow can reach values higher than the applied field. However, these situations were not necessarily associated with dynamo self-generation. In other words, flows can have very efficient field amplification factors without dynamo property (an analytic example is the case of a plane flow with diverging streamlines from a point source which would strongly amplify any toroidal magnetic field). In fact, an experimental criterion for the proximity of a dynamo threshold is still lacking. The decay time of applied magnetic field pulses has been studied by the Maryland group (Peffley et al. 2000), but in conditions where dynamo generation was not reached so it is not yet known how these decay times would diverge near onset.

2.2 Mean-Field MHD

We now discuss separately the case of the mean-field MHD approach and its consequences. The reason is that it proposes an efficient treatment of the effects of turbulence and has been very successfully used in the modelling of stellar dynamos—e.g. Dikpati and Gilman (2001). There has thus been some strong motivation to test it experimentally.

We first recall the basics of mean-field MHD, readers being referred to Moffatt (1978), Krause and Rädler (1980), Rädler and Stepanov (2006) for a more complete presentation. One splits the velocity and magnetic fields into an ensemble average and a fluctuating component: $\mathbf{u} = \overline{\mathbf{u}} + \mathbf{u}'$ and $\mathbf{B} = \overline{\mathbf{B}} + \mathbf{B}'$,

$$\partial_t \overline{\mathbf{B}} = \nabla \times (\overline{\mathbf{u}' \times \mathbf{B}'}) + \nabla \times (\overline{\mathbf{u}} \times \overline{\mathbf{B}}) + \lambda \Delta \overline{\mathbf{B}}, \tag{5}$$

where the mean electromotive force $\mathcal{E} = \overline{\mathbf{u}' \times \mathbf{B}'}$ can be computed after solving the equation for the fluctuating part of the magnetic field:

$$\partial_t \mathbf{B}' = \nabla \times (\mathbf{u}' \times \mathbf{B}') - \nabla \times \mathcal{E} + \nabla \times (\overline{\mathbf{u}} \times \mathbf{B}') + \nabla \times (\mathbf{u}' \times \overline{\mathbf{B}}) + \lambda \Delta \mathbf{B}'. \tag{6}$$

In the above equation, one then usually invokes scale separation between flow sizes at which velocity gradients are effective and the global scale at which magnetic effects are considered.

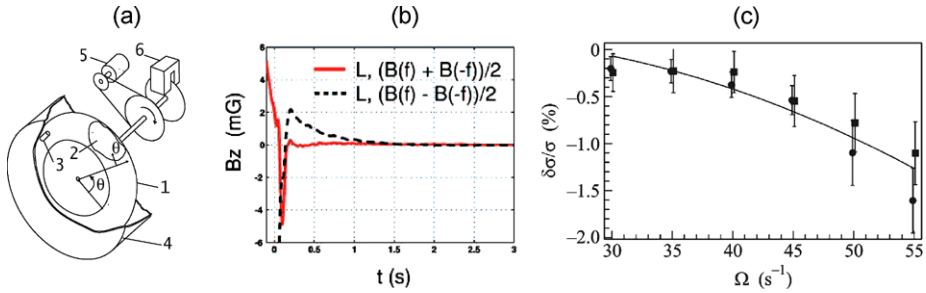

Fig. 6 Investigation of mean-field contributions. (**a**) Sketch of the Perm torus experiment (1: vessel, 2: test section, 3: Hall probe, 4: external shield, 5: motors, 6: braking device). (**b**) Study of possible α-mechanisms: response to a DC applied field with its direction parallel to the large scale helicity in the spin-down regime: the *red curve* has the symmetry of the alpha effect and is concentrated during the initial phase of motion, while the *black dashed curve* is the linear induction and follows the flow decay—figure from Stepanov et al. (2006). (**c**) Study of possible β effect, using the induction from an AC applied field. The plot shows the change in effective electrical conductivity with the initial rotation rate of the torus, from Denisov et al. (2008)

One then makes the assumption that the mean e.m.f. can be expanded in terms of the mean magnetic field $\overline{\mathbf{B}}$ and its spatial derivatives. For very general situations in the presence of a mean flow this is quite a complex task, often guided by symmetry considerations (Rädler and Stepanov 2006). Usually, the first two terms of the expansion are retained, corresponding to

- the so-called α-effect, *i.e.* the possibility to generate induced currents which are parallel to the large scale field, via an emf $\mathcal{E} = \alpha(\mathbf{u})\overline{\mathbf{B}}$. For instance, such currents have the ability to generate a poloidal magnetic field from an azimuthal one (as cooperative Parker effect from small scales), a very interesting feature for the modelization of natural dynamos.
- the 'β-effect', which corresponds to a contribution to the induced mean emf related to the gradients of $\overline{\mathbf{B}}$, $\mathcal{E} \propto \beta(\mathbf{u})(\nabla \times \overline{\mathbf{B}})$. This term represents a potential additional diffusion of the magnetic field, over the molecular Joule effect.

In cases where the flow geometry is prescribed in a simple enough form, the α term can be computed analytically. Roberts (1972) computed this α term for a flow, consisting of an array of columns in which the motions are helical with alternate axial and angular velocities, but unchanged helicity. This effect is the basis of the Karlsruhe dynamo experiment (Busse 1992; Tilgner 1997), for which both the scale separation and the helical nature of the flow are enforced by the design of the tubes that guide the flow. One can thus conclude that a cooperative effect of small-scale helical motions is experimentally observed in situations where the helical motions are strictly enforced.

The picture is somewhat different in flows where helicity evolves freely. For homogeneous (but not mirror-symmetric) turbulence, α can be computed in terms of the helicity spectrum of the flow (Moffatt 1978). For more complex geometries (in particular when mean flow motions are also present) a formal derivation of the α tensor has been performed using symmetry arguments (Rädler and Stepanov 2006). Some contributions have been tested experimentally in the Perm spin-down experiment (Frick et al. 2002; Denisov et al. 2001), displayed in Fig. 6(a): liquid Gallium is spun inside a torus which is suddenly halted; as the liquid moves with respect to the vessel, it flows past mechanical diverters which impart a global screw motion—then helicity is often assumed to cascade down to smaller scales (Chen et al. 2003). Analysis of the magnetic field induced by an applied toroidal field is shown in Fig. 6(b) where the induced field is monitored in the spin-down regime (Stepanov et al. 2006). The α value measured experimentally is much lower

than predictions derived by simple arguments of the mean-field theory based on small-scale helicity; however, it has the correct order of magnitude if one includes effects associated with the inhomogeneity of velocity gradients during spin-down (Stepanov et al. 2006). In addition, the main contribution traces back to the large scale inhomogeneity of the velocity gradients, rather than to the small scale helicity distribution.

Direct measurements of the β effect have been performed in two experiments. In a first one at very moderate turbulent Reynolds number, an increase of the molecular diffusion by a few percent has been claimed (Reighard and Brown 2001). A more recent, and far more detailed experimental study, has been performed by the Perm group. It shows a correction to the molecular magnetic diffusivity of 1% at most (Denisov et al. 2008)—Fig. 6(c). The scaling with magnetic Reynolds number was found to be in agreement with mean-field theory expressions, but the amplitude again much smaller than predicted. Finally, an indirect estimation of the effect of turbulence on magnetic diffusivity is provided by the dynamo onset in the Karlsruhe and Riga experiments: in both cases the threshold was found to be in excellent agreement with predictions based on a laminar mean flow, *i.e.* neglecting small-scale turbulent fluctuations. The field at saturation however, was observed to be in good agreement with a balance of the Lorentz force with the pressure term and turbulent fluctuations (inertial term) (Pétrélis and Fauve 2001).

There is thus experimental indications that for flows of liquid metals at moderate magnetic Reynolds numbers, the effects that can be attributed to small-scale turbulence are actually smaller than predicted by the mean-field MHD theory. It does not mean that turbulence does not play a role in experimental dynamos. On the contrary, we will show that the VKS dynamo cannot be attributed to the mean (time-averaged) flow motions. In addition, induction measurements made in the Madison experiment (Spence et al. 2006) have directly evidenced the existence of a turbulent emf: an induced dipole moment has been measured in response to an axisymmetric magnetic field—with Cowling's theorem (Cowling 1933) showing that it cannot be attributed to axisymmetric flow motions. These are indications that, at least for low P_M fluids, the turbulent and non-stationary fluctuations in the vicinity of the large scales may play a dominant role in the induction processes.

2.3 A Synthetic Dynamo

We conclude this section with an example of a dynamo based on an arrangement initially proposed by Bullard (1955), and in which the dynamo cycle is viewed as a series of magnetic induction steps. An initial magnetic seed field $\mathbf{B}_0$, transported and stretched by the velocity gradients gives rise to an induced magnetic field component $\mathbf{B}_1$, which in turn generates an induced field $\mathbf{B}_2$, etc. until eventually the contribution after n steps $\mathbf{B}_n$ reinforces $\mathbf{B}_0$ (Bourgoin et al. 2004b). If this feedback process is efficient enough, $\mathbf{B}_0$ is self-sustained (it is the neutral mode of the dynamo instability).

In the spirit of Bullard's design, we use the differential rotation in the von Kármán flow with two counter rotating disks. It advects and stretches an externally applied axial field B_z, generating a toroidal component B_θ. This induced field is used to drive a power source which generates the current in the Helmholtz coils creating B_z—cf. Fig. 7. Hence, part of the dynamo cycle is generated by an external feed-back: one prescribes the mechanism by which a toroidal magnetic field generates an induced poloidal one. The feedback loop from the induced toroidal field to the applied axial one has an adjustable gain which selects the magnetic Reynolds number for dynamo onset. The flow turbulence is included in the poloidal to toroidal conversion (ω-effect) and has a leading role. Another feature of this arrangement is that saturation of the dynamo, in its present form, is not due to the modification of the flow field, but rather to the limit value $I_{\max}$ of the currents in the external coils.

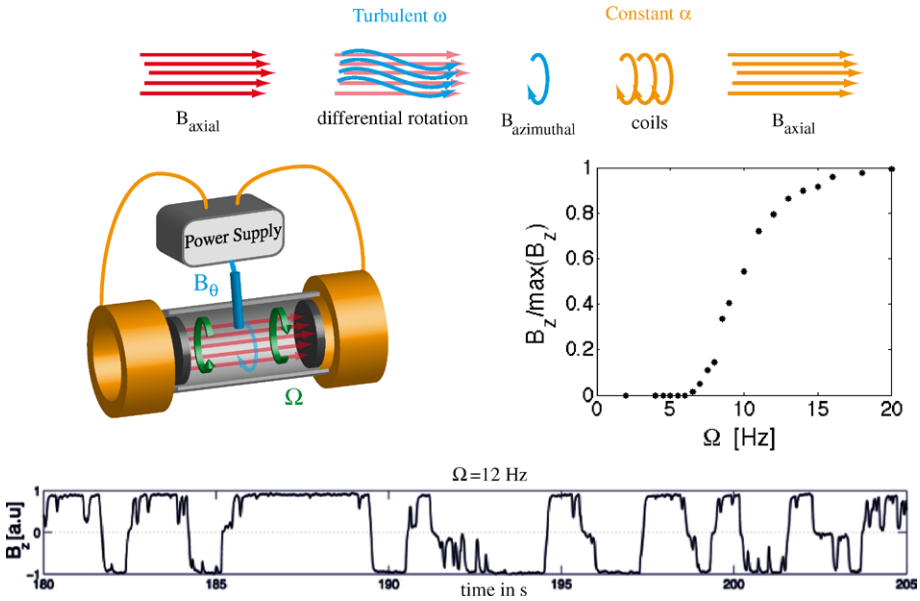

Fig. 7 The Bullard von-Kármán dynamo. (*top*): Principle of dynamo feed-back loop with actual implementation (*middle left*). The *mid-right curve* is the bifurcation curve of the self-sustained magnetic field as the rotation rate of the impellers increase. The *bottom figure* shows an example of time signal, with reversals of the dipole field, figure from Bourgoin et al. (2006)

The effect of turbulence are thus best isolated in the vicinity of onset (Bourgoin et al. 2006; Verhille et al. 2009):

(i) the bifurcation to dynamo proceeds via an on-off scenario (Sweet et al. 2001),
(ii) the bifurcation is very much dependent on the geometry and dynamics of the von Kármán flow fluctuations. Both homopolar or reversing dynamos have been observed depending on the presence of additive noise in the induction process—see Fig. 7. This is in agreement with recent models of on-off bifurcations (Aumaitre et al. 2005, 2006; Aumaitre and Pétrélis, 2006).

3 Dynamo Experiments

3.1 The Riga Experiments

The arrangement in Riga (Fig. 8(a, b)) is inspired by the Ponomarenko kinematic dynamo (Ponomarenko 1973; Gailitis and Freibergs 1976), generated by the helical motions in an infinite stationary conductor. With the first experiments made in the 80s, this swirling flow configuration has been thoroughly optimized (Gailitis 1996): back flow characteristics, addition of an external layer of sodium at rest, length of the main channel, poloidal to toroidal velocity ratio, etc. Generation and saturation of a time-dependent dynamo was first observed during summer 2000.

For a fluid in axial translation at velocity U_z while rotating at speed U_θ in a cylinder of radius R, the threshold for (Ponomarenko) self-generation in magnetic Reynolds number $R_M = R(U_\theta^2 + U_z^2)^{1/2}/\lambda$ is $R_M^c \sim 17.7$, and the bifurcation is a Hopf one: the magnetic field

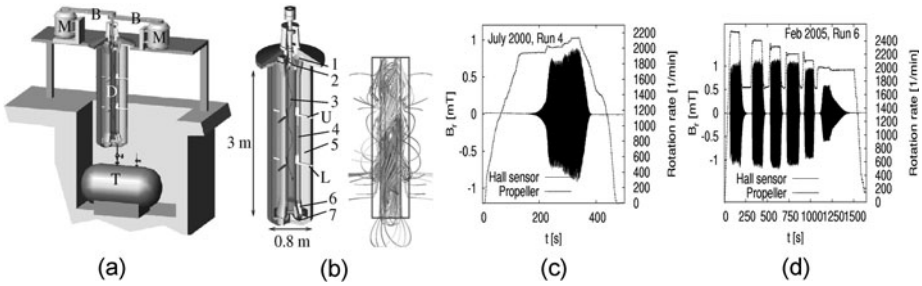

Fig. 8 The Riga dynamo experiment and its neutral mode. (**a**) Sketch of the facility. M—Motors. B—Belts. D—Central dynamo module. T—Sodium tank. (**b**) Sketch of the central module. 1—Guiding blades. 2—Propeller. 3—Helical flow region without any flow-guides, flow rotation is maintained by inertia only. 4—Back-flow region. 5—Sodium at rest. 6—Guiding blades. 7—Flow bending region. Associated simulated magnetic eigenfield. The gray scale indicates the vertical components of the field. (**c**) and (**d**): Two experimental runs carried out in July 2000 and in February 2005. Rotation rate of the motors, and magnetic field measured at one Hall external sensor plotted vs. time. Figures from Stefani et al. (2008) (Figs. 5 & 6)

at onset is oscillatory. This is very close to the threshold (17.6) observed in the experiment (Fig. 8(c, d)), with the additional following observations (Gailitis et al. 2001, 2002a, 2002b):

- optimization studies have shown that lowest threshold values are obtained when $U_\theta/U_z \sim 1$, *i.e.* for a unit ratio of 'poloidal' to 'toroidal' velocities—a feature common to all dynamo experiments so far,
- the layer of sodium at rest around the flow leads to a decrease in R_M^c,
- the main mechanism of magnetic field saturation lies in the downward breaking of the differential rotation between the innermost helical flow and the back-flow region (Gailitis et al. 2004).

3.2 The Karlsruhe Experiment

Like the previous one, the Karlsruhe experiment is designed to replicate a velocity field with a topology that is known to generate a dynamo. Here, the flow field traces back to a calculation by Roberts (1972) for a periodic array of vortices with the same helicity. This arrangement was later adapted by F. Busse for possible scenario of the Earth dynamo, a possibility that motivated the Karlsruhe experiment. In contrast to the Riga design, the Karlsruhe dynamo is a two-scale experiment. Scale separation is achieved using a quasi-periodic columnar vortex structure which forms an array of motions with like-sign helicity—this is the 'small scale' motion (Fig. 9(a)). The magnetic field, on the other hand, can develop on the larger scale of the whole experiment. In practice each of the 52 helical vortex generators is made of 2 concentric channels: one in which the flow is purely axial, and a surrounding one in which the fluid is guided in helical motion.

A very comprehensive review of the experiment and its findings can be found in Müller et al. (2006). Dynamo action was obtained for critical values of the magnetic Reynolds number $Rm^c = \alpha_\perp L/\lambda \in [8.4, 9.3]$ (here the α parameter is used as a velocity characteristic scale, and L is the overall cross-section of the experiment). This is again very close to the value (8.2) predicted using several approaches based on a laminar flow structure. One may note here again the two-scale structure of this dynamo: almost identical prediction have been obtained using the complete flow or a mean-field approach (Tilgner and Busse 2002; Rädler et al. 2002; Tilgner 2002).

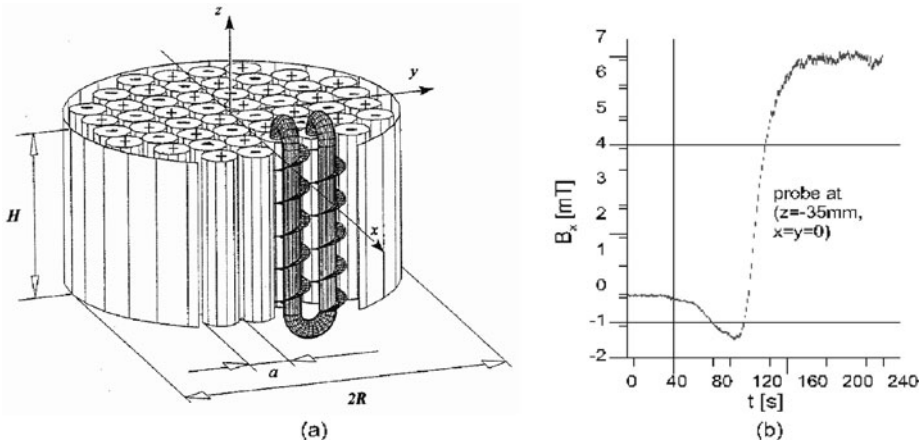

Fig. 9 The Karlsruhe dynamo experiment. (**a**) Central part of the facility. The module consists of 52 spin-generators, each containing a central tube with non-rotating flow and an outer tube where the flow is forced on a helical path. (**b**) Self-excitation and saturation in the Karlsruhe dynamo experiment. Hall sensor signals of B_x in the inner bore of the module. Figure taken from Stefani et al. (2008)

The bifurcation is supercritical, with a (statistically) stationary magnetic field generated at onset (Fig. 9(b)). The magnetic field generated is of dipolar character, oriented perpendicular to the axis of the spin generators ('an equatorial dipole'). Measurement of the pressure and flow rates in the channels indicates an additional dissipation above onset which varies linearly with the flow rate, with an order of magnitude of about 10 kW at 10% over threshold (Müller et al. 2006, 2008). As the dynamo field grows, a reduction of the flow velocity in the spin generators is also observed, however, the detailed mechanisms of the saturation of the instability are not known.

3.3 VKS Experiment

The Karlsruhe and Riga experiments have validated the principle of fluid dynamos. In each flow the kinetic Reynolds number is huge, but the overall behavior is in good agreement with the predictions of quasi-laminar approximations. They have shown that the dynamo generation is controlled by the topology and dynamics of the large scale flow. Secondary bifurcations or more complex magnetic regimes have not been observed. The VKS experiment has been designed to keep essential ingredients (shear and helicity) while at the same time allowing for more freedom to the hydrodynamic flow—and hence to the magnetic field dynamics.

The flow is generated by rotating two impellers inside a cylindrical copper vessel—details are given in Fig. 10. The impellers can be independently driven up to typically 27 Hz by motors with a total of 300 kW available power. In all configurations reported here, the impellers are manufactured from soft iron. When both impellers rotate at the same frequency $F_1 = F_2$, the forcing is symmetric with respect to any rotation R_π of π around any radial axis in its equatorial plane ($x = 0$). Otherwise, when $F_1 \neq F_2$, the system is no longer R_π-symmetric. For simplicity, we will also refer these situations as 'symmetric/asymmetric' cases.

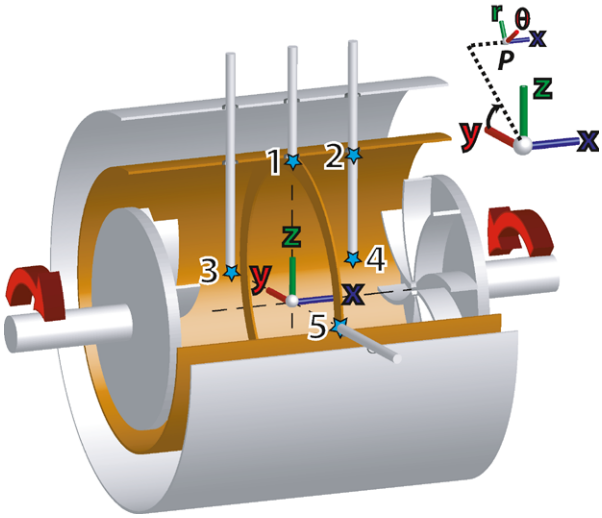

Fig. 10 Sketch of the VKS flow configuration. The flow is generated by rotating two impellers of radius 154.5 mm, 371 mm apart in a thin cylindrical copper vessel, $2R = 412$ mm in inner diameter and 524 mm in length. The impellers are fitted with 8 curved blades of height $h = 41.2$ mm; in most experimental runs, the impellers are rotated so that the blades move in a 'non-scooping' direction, defined as the positive direction by arrows. The flow is surrounded by sodium at rest contained in another concentric cylindrical copper vessel, 578 mm in inner diameter and 604 mm long. An oil circulation in this thick copper vessel maintains a regulated temperature in the range 110–160°C. In the mid plane between the impellers one can attach a thin annulus inner diameter 350 mm and thickness 5 mm. The impellers that generate the flow have been machined from pure soft iron ($\mu_r \sim 100$). Positions 1 to 5 correspond to points where time recordings of the magnetic field have been made, using 3D Hall probes. Figure from Monchaux et al. (2009)

3.3.1 A Statistically Steady Turbulent Dynamo

For symmetric forcing, one observes that, as the rotation rate of the impellers $F = F_1 = F_2$ is increased above 17 Hz, the magnetic field inside the flow develops strong fluctuations and its main component (in the azimuthal direction at the probe location) grows and saturates to a mean values up to 100 G—Fig. 11. This value is about 100 times larger than the ambient magnetic field in the experimental hall, from which the flow volume is not shielded. The hundred-fold increase is also one order of magnitude larger than the induction effects and field amplification previously recorded in the VKS experiment with externally applied magnetic field, either homogeneously over the flow volume (Bourgoin et al. 2002) or localized at the flow boundary (Volk et al. 2006a). The most salient features of the dynamo observed with a symmetric forcing are the following (Monchaux et al. 2007, 2009; Aumaître et al. 2008):

- it appears via a supercritical bifurcation at $R_M^c \sim 32$, generating a statistically steady magnetic field,
- the geometry of the dynamo field is mainly that of an axial dipole,
- opposite polarities of the dipole have been observed as R_M is increased above threshold (in agreement with the expected $\mathbf{B} \to -\mathbf{B}$ symmetry of the equations) but once a direction of the dipole has been chosen at onset, no secondary bifurcation is observed as R_M is increased to its maximum accessible value ($R_M^{\max} \sim 50$),
- the amplitude of the field at saturation is in good agreement with a balance of the Lorentz force with the non-linear term in the Navier-Stokes equation (Pétrélis and Fauve 2001).

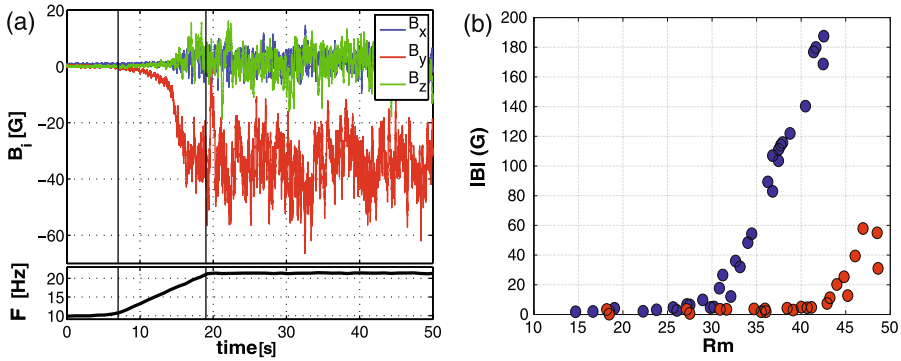

Fig. 11 Self-generation in the VKS experiment. (**a**) Growth of the magnetic field as the rotation rate of the impellers $F = F_1 = F_2$ is increased from 10 to 22 Hz. Three components of the magnetic field recorded at location 1. (**b**) Magnetic field amplitude $\langle B^2 \rangle^{1/2}$ recorded at location 3; (*blue circles*): counter-rotating impellers at equal rotation rates, in the positive direction shown in Fig. 9. (*red circles*): Impellers counter-rotating in the opposite direction, i.e. with the blades on the impellers moving in a 'scooping' or negative direction. Changes in the efficiency of the stirring are taken into account in the definition of R_M; $R_M = K\mu_0\sigma R^2 F$ with $K = K+ = 0.6$ in the normal, positive direction of rotation and $K = K- = 0.7$ in the opposite direction. Figure from Monchaux et al. (2009)

The observation that the magnetic field geometry for the symmetric VKS forcing is mainly dipolar has important implications. It strongly differs from the prediction of kinematic calculations based on the topology of the mean von Kármán flow which tends to favor a transverse dipole (Marié et al. 2003; Ravelet et al. 2005; Bourgoin et al. 2004b). In addition, Cowling theorem (Moffatt 1978) implies that it has not been generated by the mean flow motions alone. The axial symmetry, however, is what would be expected from an $\alpha - \omega$ dynamo. The differential rotation induced by the counter-rotation of the impellers has the ability to generate an azimuthal field component from an axial magnetic field (Bourgoin et al. 2002, 2004a). The conversion by the α-effect of a toroidal field into a poloidal one is often thought to rely on helical flow motions, but the source of the α term in VKS is yet unclear. Several mechanisms have been proposed (Laguerre et al. 2008; Monchaux et al. 2009) and further measurements are underway. A point which deserves clarification concerns the role of the ferromagnetic impellers which are used to drive the flow. Dynamo action has not been reached in identical conditions for impellers manufactured from stainless steel instead of soft iron. Further studies will have to establish (i) whether the use of iron impellers only lowers the threshold of the same dynamo that would exist with non-ferromagnetic drives, (ii) if, instead, the modification of the boundary conditions favor an axisymmetric mode compared to the equatorial dipole predicted from kinematic dynamo simulations based on the time-averaged flow; (iii) more generally, the role of high permeability of the impellers on the generation of a poloidal magnetic field from a toroidal component induced by differential rotation.

3.3.2 Dynamical Regimes for an Asymmetric Forcing

When the flow is forced with the impellers rotating at different rates, studies in water-prototypes have shown that global rotation is imparted to the flow (Marié 2003; Monchaux 2007): there are strong similarities between the von Kármán flow forced by impellers rotating respectively at F_1 and F_2 in the laboratory frame or by impellers rotating at $(F_1 + F_2)/2$

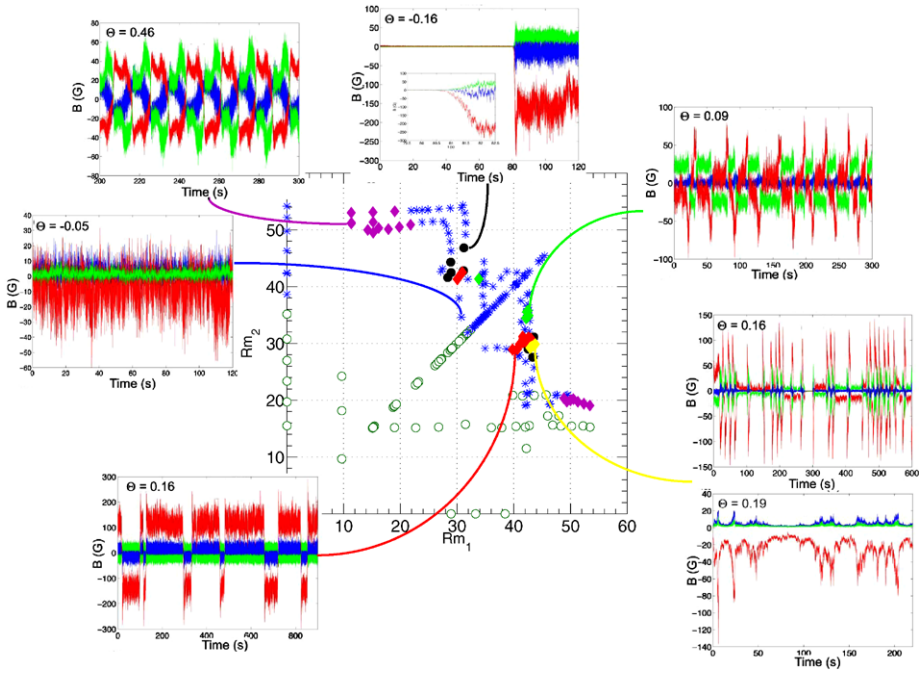

Fig. 12 Dynamical regimes observed in the von Kármán sodium experiment when the impellers driving the flow rotate at varying rates: the coordinates in the main plot are the magnetic Reynolds numbers built from the velocity of each impeller. The *insets* give examples of time signals of the 3 components of the magnetic field recorded in the mid-plane of the cylinder. Figure extracted from data in Monchaux et al. (2009)

in a frame rotating at $(F_1 - F_2)/2$. In addition, this asymmetric differential forcing brakes the R_π symmetry.

The added degree of freedom gives access to a variety of dynamos with complex dynamical regimes—they are shown in Fig. 12 using two independent Reynolds numbers built on the rotation rates of each impeller (Monchaux et al. 2009). Regions where (statistically) stationary dynamos are generated alternate with regions for which the magnetic field is time dependent. Of particular interest is the region near $|\theta| \equiv 2|F_1 - F_2|/(F_1 + F_2) = 0.16$ where reversals of the dipole field are observed at irregular time intervals. This regime, which also includes excursions, bears some similarity with the behavior of the geodynamo (Berhanu et al. 2007). Another very intriguing regime is reached in the same region where the dynamo has sudden 'bursts' between high and low fields states—Fig. 12 (right part). Both regimes are observed in a region where the flow has also two possible states (Monchaux et al. 2006; Ravelet et al. 2008).

Further studies (Monchaux et al. 2008) have shown that these regimes can be interpreted as the development and interaction of few dynamo modes (essentially a dipole and a quadrupole) when the flow is forced asymmetrically. The proximity of dipole and quadrupole modes in $\alpha - \omega$ dynamos has been pointed out by many numerical studies (Kutzner and Christensen 2004; Morin 2004), and few-modes interactions have long been used to ascribe dynamical features to the dynamo instability (Nozières 1978). For the case of the VKS dynamos, the onset of oscillatory behavior and the occurrence of random reversals, have recently been described using a low dimensional model (Pétrélis and Fauve 2008).

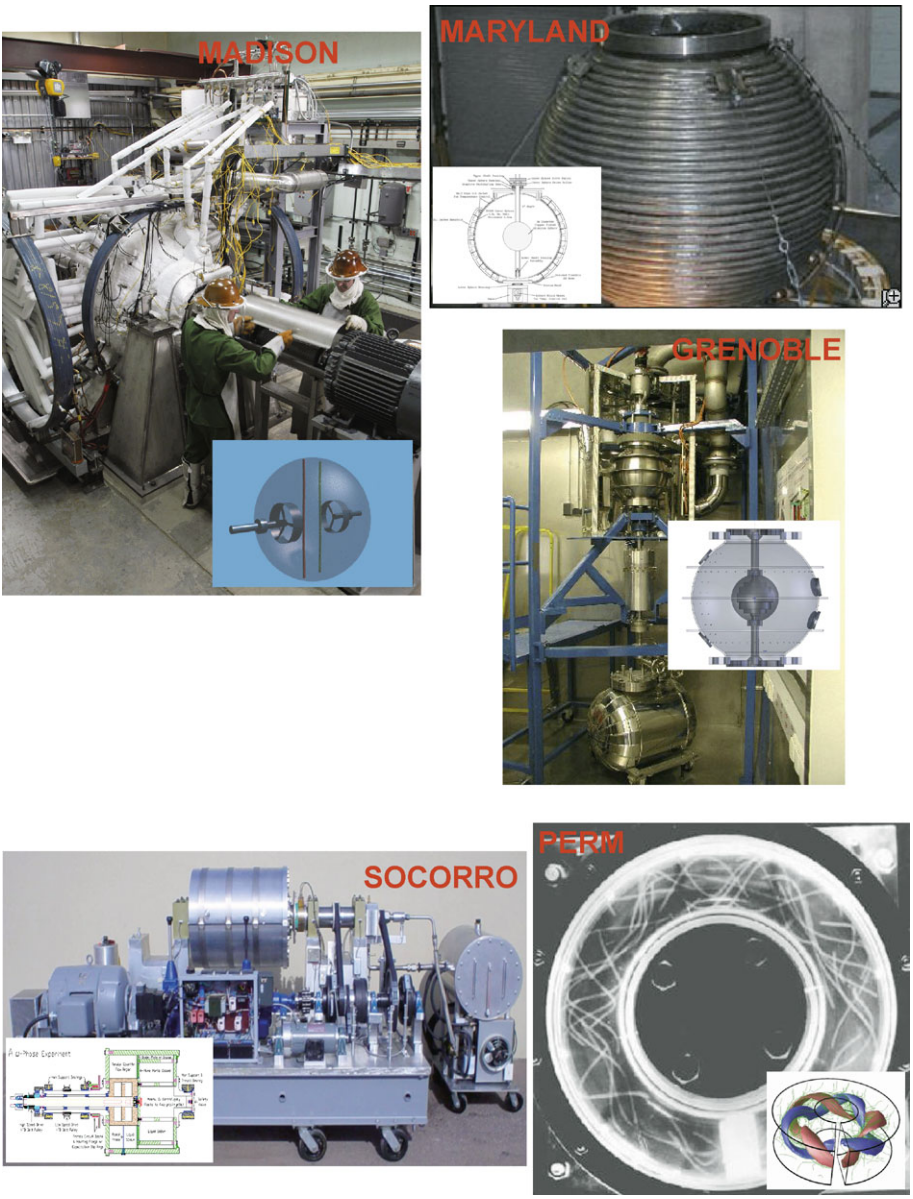

Fig. 13 Other sodium experiments operated or in preparation, aimed at studying the dynamo instability. Starting from top/left and clockwise: the Madison dynamo experiment at Univ. Wisconsin, USA; the 3-Meter system being installed at University of Maryland, USA; the DTS spherical Couette flow of the Grenoble team, France; the spin-down helical flow in the Perm torus, Russia; the cylindrical Couette flow in Socorro, New Mexico, USA

3.4 Related Dynamo Experiments

Several other experiments, shown in Fig. 13, are operated or in preparation world-wide.

- A setup similar to the VKS arrangement, but in a spherical volume, is studied by the group of Cary Forest at University of Wisconsin (USA). It has shown the possibility that turbulent motions induce an axial dipole from an applied external field (Spence et al. 2006).
- The Complex Dynamics group headed by Daniel Lathrop at University of Maryland (USA) has operated a large variety of sodium experiments, showing in particular the influence of the driving on the induction efficiency (Peffley et al. 2000). The most recent developments have been made in spherical Couette flows with applied magnetic fields, showing coupled flow and magnetic field patterns consistent with a magneto-rotational instability (Sisan et al. 2004). A large spherical Couette experiment (with an outer sphere 3 meters in diameter) is planned; it will reach the highest accessible magnetic Reynolds numbers of all current experiments.
- A spherical Couette experiment is run in Grenoble (France) by the group of H.-C. Nataf, D. Jault and Ph. Cardin. The inner sphere contains a strong permanent magnet with the purpose of studying flows and magnetic regimes in conditions closer to the ones that prevail in the Earth. The first measurements have evidenced a large variety of magneto-inertial waves (Schmitt et al. 2008).
- At the Institute for Continuous Media Mechanics in Perm (Russia), the team of Peter Frick has designed a spin-down helical flow inside a torus (Frick et al. 2002; Denisov et al. 2001). Compared to other experiments the flow is strongly non-stationary: a strongly anisotropic turbulence develops and decays, as the fast-rotating torus is suddenly put to halt (Noskov et al. 2009). This flow has the potential to sustain a dynamo in the transient relaxation, and repeated realizations are expected to help understand the magnetic-velocity field interactions during the phases of growth, saturation and decay.
- In Socorro (New Mexico, USA), the team led by Stirling Colgate has designed a Couette flow operated with sodium, with the aim of generating an $\alpha\omega$ dynamo. Characterization of hydrodynamic flow transition have been carried out (Beckley 2002).

There are also several experiments intended to study the Magneto-Rotational Instability (MRI) in Couette flows. One is developed in Obninsk (Russia), in collaboration with the Kurchatov Institute in Moscow (Velikhov 2006). Another is in Rossendorf, operated by the group of Gunter Gerbeth and Frank Stefani. This experiment has recently shown an MRI in the form of a travelling wave (Stefani et al. 2007).

4 Concluding Remarks

Several features are shared by experimental dynamos operated so far with progressively less constrained motions—since the pioneering works of Lowes and Wilkinson in Cambridge in the 60s. All have observed that the bifurcations is supercritical, and subcritical bifurcation are yet to be evidenced experimentally. Boundary conditions have been essential, particularly in order to shift the critical magnetic Reynolds number R_M^c within the range accessible in the chosen experimental devices. Much further studies are necessary in order to understand the role of turbulence in the generation of the magnetic field and its saturation. With a growing number of dynamo experiments worldwide, and with the narrowing gap with numerical simulations, the next decade appears very promising.

Acknowledgements The authors gratefully acknowledge the contribution of an anonymous referee. Bullard-von Kármán and standard von Kármán experiments are operated at ENS-Lyon. The von Kármán Sodium experiments are designed and run by the VKS collaboration on the premises of the CEA—

Direction de l'Energie Nucléaire in Cadarache. The VKS team includes François Daviaud, Arnaud Chiffaudel, Sébastien Aumaître, Bérengère Dubrulle, Florent Ravelet, Romain Monchaux, Louis Marié at CEA—Département de Sciences de la Matière; Stephan Fauve, François Pétrélis, Nicolas Mordant, Michael Berhanu at Ecole Normale Supérieure de Paris and Jean-François Pinton, Philippe Odier, Mickael Bourgoin, Romain Volk, Nicolas Plihon at Ecole Normale Supérieure de Lyon. Fruitful discussions with members of the VKS team are gratefully acknowledged.

This work was supported by CEA, CNRS and ANR NT05-1 42110, ANR-08-BLAN-0039-02.

References

MHD dynamo experiments. Magnetohydrodynamics **38**(1/2) (2002), special issue

J.-F. Pinton, R. Moreau (eds.), The dynamo effect, experimental progress, geo and astrophysical challenges. C.R. Acad. Sci. **9**(7) (2008)

S. Aumaitre, F. Pétrélis, Modification of instability processes by multiplicative noises. Eur. J. Phys. B **51**, 357 (2006)

S. Aumaitre, F. Pétrélis, K. Mallick, Low frequency noise controls on-off intermittency of bifurcating systems. Phys. Rev. Lett. **95**, 064101 (2005)

S. Aumaitre, K. Mallick, F. Pétrélis, Effects of the low frequencies of noise on on-off-bifurcations. J. Stat. Phys. **123**, 909 (2006)

S. Aumaître, M. Berhanu, M. Bourgoin, A. Chiffaudel, F. Daviaud, B. Dubrulle, S. Fauve, L. Marié, R. Monchaux, N. Mordant, Ph. Odier, F. Pétrélis, J.-F. Pinton, N. Plihon, F. Ravelet, R. Volk, The VKS experiment: turbulent dynamical dynamos. C.R. Acad. Sci. **9**(7), 689 (2008)

R. Avalos-Zuniga, F. Plunian, Influence of inner and outer walls electromagnetic properties on the onset of a stationary dynamo. Eur. Phys. J. B **47**(1), 127 (2005)

H.F. Beckley, Measurement of annular Couette flow stability at the fluid Reynolds number $Re = 4.4\ 10^6$: the fluid dynamic precursor to a liquid sodium $\alpha\omega$ dynamo. PhD Dissertation, New Mexico Institute of Mining and Technology, 2002

M. Berhanu, R. Monchaux, M. Bourgoin, M. Moulin, Ph. Odier, J.-F. Pinton, R. Volk, S. Fauve, N. Mordant, F. Pétrélis, A. Chiffaudel, F. Daviaud, B. Dubrulle, C. Gasquet, L. Marié, F. Ravelet, Magnetic field reversals in an experimental turbulent dynamo. Europhys. Lett. **77**, 59007 (2007)

M. Bourgoin, Etudes en magnétohydrodynamique, application à l'effet dynamo. PhD Thesis, Ecole Normale Supérieure de Lyon, 2003. http://tel.archives-ouvertes.fr/tel-00008302/en/

M. Bourgoin, L. Marié, F. Pétrélis, C. Gasquet, A. Guigon, J.-B. Luciani, M. Moulin, F. Namer, J. Burguete, A. Chiffaudel, F. Daviaud, S. Fauve, Ph. Odier, J.-F. Pinton, Magnetohydrodynamics measurements in the von Kármán sodium experiment. Phys. Fluids **14**, 3046–3058 (2002)

M. Bourgoin, R. Volk, P. Frick, S. Kripechenko, P. Odier, J.-F. Pinton, Induction mechanisms in von Kármán swirling flows of liquid Gallium. Magnetohydrodynamics **40**(1), 13–31 (2004a)

M. Bourgoin, P. Odier, J.-F. Pinton, Y. Ricard, An iterative study of time independent induction effects in magnetohydrodynamics. Phys. Fluids **16**(7), 2529–2547 (2004b)

M. Bourgoin, R. Volk, N. Plihon, P. Augier, Ph. Odier, J.-F. Pinton, A Bullard von Kármán dynamo. New J. Phys. **8**, 329 (2006)

E.C. Bullard, The stability of a homopolar dynamo. Proc. Camb. Philos. Soc. **51**, 744 (1955)

E.C. Bullard, D. Gubbins, Generation of magnetic fields by fluid motions of global scale. Geophys. Astrophys. Fluid Dyn. **8**, 43 (1977)

F.H. Busse, Dynamo theory of planetary magnetism and laboratory experiments, in *Evolution of Dynamical Structures in Complex Systems*, ed. by R. Friedrich, A. Wunderlin (Springer, Berlin, 1992), pp. 359–384

Q.N. Chen, S.Y. Chen, G.L. Eyink, The joint cascade of energy and helicity in three-dimensional turbulence. Phys. Fluids **15**(2), 361–374 (2003)

T.G. Cowling, The magnetic field of sunspots. Mon. Not. R. Astron. Soc. **94**, 39 (1933)

S. Denisov, V. Noskov, A. Sukhanovskiy, P. Frick, Unsteady turbulent spiral flows in a circular channel. Fluid Dyn. **36**(5), 734–742 (2001)

S.A. Denisov, V.I. Noskov, R.A. Stepanov, P.G. Frick, Measurements of turbulent magnetic diffusivity in a liquid-Gallium flow. JETP Lett. **88**(3), 167–171 (2008)

M. Dikpati, P.A. Gilman, Flux-transport dynamos with α-effect from global instability of tachocline differential rotation: a solution for magnetic parity selection in the sun. Astrophys. J. **559**(1), 428–442 (2001)

N.L. Dudley, R.W. James, Time-dependent kinematic dynamos with stationary flows. Proc. R. Soc. Lond. Ser. A **425**, 407 (1989)

P. Frick, V. Noskov, S. Denisov, S. Khripchenko, D. Sokoloff, R. Stepanov, A. Sukhanovsky, Non-stationary screw flow in a toroidal channel: way to a laboratory dynamo experiment. Magnetohydrodynamics **38**, 136–155 (2002)

A. Gailitis, Project of a liquid sodium MHD dynamo experiment. Magnetohydrodynamics **32**, 58–62 (1996)
A. Gailitis, Ya. Freibergs, Theory of a helical MHD dynamo. Magnetohydrodynamics **12**, 127–129 (1976)
A. Gailitis, O. Lielausis, S. Dement'ev, E. Platacis, A. Cifersons, G. Gerbeth, T. Gundrum, F. Stefani, M. Christen, H. Hänel, G. Will, Detection of a flow induced magnetic field eigenmode in the Riga dynamo facility. Phys. Rev. Lett. **84**(19), 4365 (2000)
A. Gailitis et al., Magnetic field saturation in the Riga dynamo experiment. Phys. Rev. Lett. **86**, 3024–3027 (2001)
A. Gailitis, O. Lielausis, E. Platacis, G. Gerbeth, F. Stefani, On back-reaction effects in the Riga dynamo experiment. Magnetohydrodynamics **38**, 15–26 (2002a)
A. Gailitis, O. Lielausis, E. Platacis, G. Gerbeth, F. Stefani, *Colloquium*: Laboratory experiments on hydromagnetic dynamos. Rev. Mod. Phys. **74**, 973–990 (2002b)
A. Gailitis, O. Lielausis, E. Platacis, G. Gerbeth, F. Stefani, The Riga dynamo experiment. Surv. Geophys. **24**(3), 247–267 (2003)
A. Gailitis, O. Lielausis, E. Platacis, G. Gerbeth, F. Stefan, Riga dynamo experiment and its theoretical background. Phys. Plasmas **11**(5), 2838 (2004)
C. Gissinger, A. Iskakov, S. Fauve, E. Dormy, Effect of magnetic boundary conditions on the dynamo threshold of von Karman swirling flows. Europhys. Lett. **82**(2), 29001 (2008)
D.H. Kelley, S.A. Triana, D.S. Zimmerman, A. Tilgner, D.P. Lathrop, Inertial waves driven by differential rotation in a planetary geometry. GAFD **101**(5–6), 469–487 (2007)
F. Krause, K.-H. Rädler, *Mean Field Magnetohydrodynamics and Dynamo Theory* (Pergamon Press, New York, 1980)
C. Kutzner, U.R. Christensen, Simulated geomagnetic reversals and preferred virtual geomagnetic pole paths. Geophys. J. Int. **157**(3), 1105–118 (2004)
R. Laguerre, C. Nore, A. Ribeiro, J. Leorat, J.L. Guermond, F. Plunian, Impact of impellers on the axisymmetric magnetic mode in the VKS2 dynamo experiment. Phys. Rev. Lett. **101**(10), 104501 (2008), correction in Phys. Rev. Lett. **101**(21), 219902 (2008)
F.J. Lowes, I. Wilkinson, Geomagnetic dynamo: a laboratory model. Nature **198**, 1158–1160 (1963)
F.J. Lowes, I. Wilkinson, Geomagnetic dynamo: an improved laboratory model. Nature **219**, 717–718 (1968)
L. Marié, J. Burguete, F. Daviaud, J. Léorat, Numerical study of homogeneous dynamo based on experimental von Kármán type flows. Eur. Phys. J. B **33**, 469–485 (2003)
L. Marié, Transport de moment cinétique et de champ magnétique par un écoulement tourbillonnaire turbulent: influence de la rotation. PhD thesis, Université de Paris 7, 2003. http://tel.archives-ouvertes.fr/tel-00007755/en/
A. Martin, P. Odier, J.-F. Pinton, S. Fauve, Effective permeability in a binary flow of liquid gallium and iron beads. Eur. Phys. J. B **18**, 337–341 (2000)
H.K. Moffatt, *Magnetic Field Generation in Electrically Conducting Fluids* (Cambridge University Press, Cambridge, 1978)
R. Monchaux, Mécanique statistique et effet dynamo dans un écoulement de von Kármán turbulent. PhD thesis Université Diderot, Paris 7, 2007. http://tel.archives-ouvertes.fr/tel-00199751/en/
R. Monchaux, F. Ravelet, B. Dubrulle, F. Daviaud, Properties of steady states in turbulent axisymmetric flows. Phys. Rev. Lett. **96**(12), 124502 (2006)
R. Monchaux, M. Berhanu, M. Bourgoin, M. Moulin, Ph. Odier, J.-F. Pinton, R. Volk, S. Fauve, N. Mordant, F. Pétrélis, A. Chiffaudel, F. Daviaud, B. Dubrulle, C. Gasquet, L. Marié, F. Ravelet, Generation of magnetic field by dynamo action in a turbulent flow of liquid sodium. Phys. Rev. Lett. **98**, 044502 (2007)
R. Monchaux, M. Berhanu, S. Aumaître, A. Chiffaudel, F. Daviaud, B. Dubrulle, F. Ravelet, M. Bourgoin, Ph. Odier, J.-F. Pinton, N. Plihon, R. Volk, S. Fauve, N. Mordant, F. Pétrélis, Chaotic dynamos generated by a turbulent flow of liquid sodium. Phys. Rev. Lett. **101**, 074502 (2008)
R. Monchaux, M. Berhanu, S. Aumaître, A. Chiffaudel, F. Daviaud, B. Dubrulle, L. Marié, F. Ravelet, S. Fauve, N. Mordant, F. Pétrélis, M. Bourgoin, P. Odier, J.-F. Pinton, N. Plihon, R. Volk, The VKS experiment: turbulent dynamical dynamos. Phys. Fluids **21**, 035108 (2009)
N. Mordant, J.-F. Pinton, F. Chilla, Characterization of turbulence in a closed flow. J. Phys. II (France) **7**(11), 1729 (1998)
V. Morin, Instabilités et bifurcations associées à la modélisation de la géodynamo. PhD thesis, Université Diderot, Paris 7, 2004. http://tel.archives-ouvertes.fr/tel-00011484/fr/
U. Müller, R. Stieglitz, S. Horanyi, Experiments at a two-scale dynamo test facility. J. Fluid Mech. **552**, 419 (2006)
U. Müller, R. Steiglitz, F.H. Busse, A. Tilgner, The Karlsruhe two-scale dynamo experiment. C.R. Phys. **9**, 729–740 (2008)
V. Noskov, R. Stepanov, S. Denisov, P. Frick, G. Verhille, N. Plihon, J.-F. Pinton, Dynamics of a turbulent spin-down flow inside a torus. Phys. Fluids **21**, 045108 (2009)

Ph. Nozières, Reversals of the Earth's magnetic field: an attempt at a relaxation model. Phys. Earth Planet. Inter. **17**, 55–74 (1978)
P. Odier et al., Advection of a magnetic field by a turbulent swirling flow. Phys. Rev. E **58**(6), 7397–7401 (1998)
P. Odier, J.-F. Pinton, S. Fauve, Magnetic induction by coherent vortex motion. Eur. Phys. J. B **16**, 373 (2000)
E.N. Parker, Hydromagnetic dynamo models. Astrophys. J. **122**, 293 (1955)
N.L. Peffley, A.B. Cawthorne, D.P. Lathrop, Toward a self-generating magnetic dynamo: The role of turbulence. Phys. Rev. E **61**(5), 5287 (2000)
F. Pétrélis, S. Fauve, Saturation of the magnetic field above the dynamo threshold. Eur. Phys. J. B **22**, 273–276 (2001)
F. Pétrélis, S. Fauve, Chaotic dynamics of the magnetic field generated by dynamo action in a turbulent flow. J. Phys., Condens. Matter **20**, 494203 (2008)
F. Pétrélis, M. Bourgoin, L. Marié, A. Chiffaudel, S. Fauve, F. Daviaud, P. Odier, J.-F. Pinton, Non linear induction in a swirling flow of liquid sodium. Phys. Rev. Lett. **90**(17), 174501 (2003)
F. Pétrélis, N. Mordant, S. Fauve, On the magnetic fields generated by experimental dynamos. Geophys. Astrophys. Fluid Dyn. **101**(3–4), 289 (2007)
J.-F. Pinton, F. Plaza, L. Danaila, P. Le Gal, F. Anselmet, On velocity and passive scalar scaling laws in a turbulent swirling flow. Physica D **122**(1–4), 187 (1998)
Yu.B. Ponomarenko, Theory of the hydromagnetic generator. J. Appl. Mech. Tech. Phys. **14**, 775–779 (1973)
K.-H. Rädler, M. Rheinhardt, E. Apstein, On the mean-field theory of the Karlsruhe dynamo experiment I. Kinematic theory. Magnetohydrodynamics **38**, 41–71 (2002)
K.H. Rädler, R. Stepanov, Mean electromotive force due to turbulence of a conducting fluid in the presence of mean flow. Phys. Rev. E **73**(5), 056311 (2006)
F. Ravelet, A. Chiffaudel, F. Daviaud, J. Léorat, Toward an experimental von Kármán dynamo: Numerical studies for an optimized design. Phys. Fluids **17**, 117104 (2005)
F. Ravelet, R. Volk, A. Chiffaudel, F. Daviaud, B. Dubrulle, R. Monchaux, M. Bourgoin, P. Odier, J.-F. Pinton, M. Berhanu, S. Fauve, N. Mordant, F. Petrelis, Magnetic induction in a turbulent flow of liquid sodium: mean behaviour and slow fluctuations. arXiv:0704.2565 (2007)
F. Ravelet, A. Chiffaudel, F. Daviaud, Supercritical transition to turbulence in an inertially driven von Karman closed flow. J. Fluid Mech. **601**, 339 (2008)
A.B. Reighard, M.R. Brown, Turbulent conductivity measurements in a spherical liquid sodium flow. Phys. Rev. Lett. **86**(13), 2794 (2001)
G.O. Roberts, Dynamo action of fluid motions with two-dimensional periodicity. Philos. Trans. R. Soc. Lond. A **271**, 411–454 (1972)
A.A. Schekochihin, E.L. Haugen, A. Brandenburg, C. Cowley, J.L. Maron, J.C. McWilliiam, The onset of small scale turbulent dynamo at low magnetic Prandtl numbers. Astrophys. J. **625**, 115 (2004)
D. Schmitt, T. Alboussiere, D. Brito, P. Cardin, N. Gagniere, D. Jault, H.-C. Nataf, Rotating spherical Couette flow in a dipolar magnetic field: experimental study of magneto-inertial waves. J. Fluid Mech. **604**, 175–197 (2008)
C. Simand, F. Chillà, J.-F. Pinton, Study of inhomogeneous turbulence in the closed flow between corotating disks. Europhys. Lett. **49**, 336 (2000)
D. Sisan et al., Experimental observation and characterization of the magnetorotational instability. Phys. Rev. Lett. **93**(11), 114502 (2004)
E.J. Spence, M.D. Nornberg, C.M. Jacobson, R.D. Kendrick, C.B. Forest, Observation of a turbulence-induced large scale magnetic field. Phys. Rev. Lett. **96**, 055002 (2006)
E.J. Spence, K. Reuter, C.B. Forest, A spherical plasma dynamo experiment. arXiv:0901.3406 (2009)
M. Steenbeck et al., Experimental discovery of the electromotive force along the external magnetic field induced by a flow of liquid metal (α-effect). Sov. Phys. Dokl. **13**, 443 (1968)
F. Stefani, M. Xu, G. Gerbeth, F. Ravelet, A. Chiffaudel, F. Daviaud, J. Léorat, Ambivalent effects of added layers on steady kinematic dynamos in cylindrical geometry: application to the VKS experiment. Eur. J. Mech. B, Fluids **25**(6), 894 (2006)
F. Stefani, T. Gundrum, G. Gerbeth, G. Rüdiger, J. Szklarski, R. Hollerbach, Experiments on the magnetorotational instability in helical magnetic fields. New J. Phys. **9**, 295 (2007)
F. Stefani, A. Gailitis, G. Gerbeth, Magnetohydrodynamic experiments on cosmic magnetic fields. Z. Angew. Math. Mech. **88**, 930 (2008)
R. Stepanov, R. Volk, S. Denisov, P. Frick, V. Noskov, J.-F. Pinton, Induction, helicity and alpha effect in a toroidal screw flow of liquid gallium. Phys. Rev. E **73**, 046310 (2006)
D. Sweet, E. Ott, J.M. Finn, T.M. Antonsen Jr., D.P. Lathrop, Blowout bifurcations and the onset of magnetic activity in turbulent dynamos. Phys. Rev. E **63**, 066211 (2001)
A. Tilgner, A kinematic dynamo with a small scale velocity field. Phys. Lett. A **226**, 75–79 (1997)

A. Tilgner, Numerical simulation of the onset of dynamo action in an experimental two-scale dynamo. Phys. Fluids **14**, 4092–4094 (2002)

A. Tilgner, F.H. Busse, Simulation of the bifurcation diagram of the Karlsruhe dynamo. Magnetohydrodynamics **38**, 35–40 (2002)

E.P. Velikhov, Magneto-rotational instability in differentially rotating liquid metals. Phys. Lett. A. **356**, 216–221 (2006)

G. Verhille, N. Plihon, G. Fanjat, R. Volk, M. Bourgoin, J.-F. Pinton, Large scale fluctuations and dynamics of the Bullard-von Kármán dynamo. Geophys. Astrophys. Fluid Dyn. (2009, submitted)

R. Volk, R. Monchaux, M. Berhanu, F. Ravelet, A. Chiffaudel, F. Daviaud, B. Dubrulle, S. Fauve, N. Mordant, Ph. Odier, F. Pétrélis, J.-F. Pinton, Transport of magnetic field by a turbulent flow of liquid sodium. Phys. Rev. Lett. **97**, 074501 (2006a)

R. Volk, Ph. Odier, J.-F. Pinton, Fluctuation of magnetic induction in von Karman swirling flows. Phys. Fluids **18**(8), 085105 (2006b)

N.O. Weiss, The expulsion of magnetic flux by eddies. Proc. R. Soc. Lond., Ser. A **293**, 310 (1966)

M. Xu, F. Stefani, G. Gerbeth, The integral equation approach to kinematic dynamo theory and its application to dynamo experiments in cylindrical geometry. J. Comput. Phys. **227**(17), 8130 (2008)

P.J. Zandbergen, D. Dijkstra, Von Kármán swirling flows. Annu. Rev. Fluid Mech. **19**, 465 (1987), and references therein